

Dropping Anchor and Spherical Harmonics for Sparse-view Gaussian Splatting

Shuangkang Fang¹, I-Chao Shen², Xuanyang Zhang³, Zesheng Wang¹, Yufeng Wang¹,
Wenrui Ding¹, Gang Yu³, Takeo Igarashi²
¹Beihang University ²The University of Tokyo ³StepFun

<https://sk-fun.fun/DropAnSH-GS>

Abstract

Recent 3D Gaussian Splatting (3DGS) Dropout methods address overfitting under sparse-view conditions by randomly nullifying Gaussian opacities. However, we identify a neighbor compensation effect in these approaches: dropped Gaussians are often compensated by their neighbors, weakening the intended regularization. Moreover, these methods overlook the contribution of high-degree spherical harmonic coefficients (SH) to overfitting. To address these issues, we propose DropAnSH-GS, a novel anchor-based Dropout strategy. Rather than dropping Gaussians independently, our method randomly selects certain Gaussians as anchors and simultaneously removes their spatial neighbors. This effectively disrupts local redundancies near anchors and encourages the model to learn more robust, globally informed representations. Furthermore, we extend the Dropout to color attributes by randomly dropping higher-degree SH to concentrate appearance information in lower-degree SH. This strategy further mitigates overfitting and enables flexible post-training model compression via SH truncation. Experimental results demonstrate that DropAnSH-GS substantially outperforms existing Dropout methods with negligible computational overhead, and can be readily integrated into various 3DGS variants to enhance their performances.

1. Introduction

Realistic novel view synthesis (NVS) remains a central challenge in computer vision and graphics. 3DGS [25], with a remarkable balance between rendering speed and visual fidelity, has recently emerged as the leading method in this domain [5, 12, 23, 34, 51]. Although 3DGS excels in dense input views [2, 6, 21, 30, 31, 61], it faces significant challenges when trained with sparse views [9, 13, 16, 20, 37, 63]. The scarcity of training views often induces severe overfitting, manifesting as artifacts, blurring, or geometric

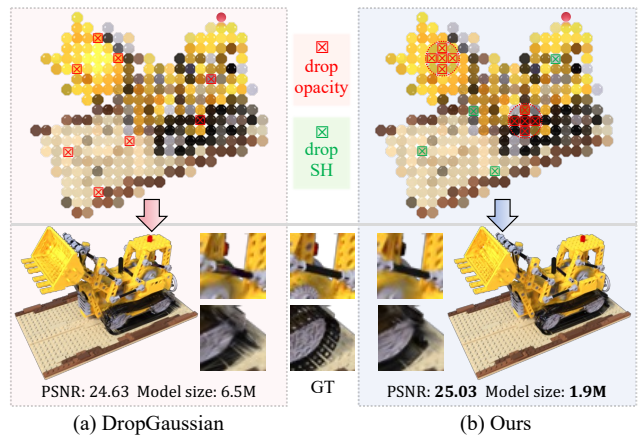


Figure 1. **Difference between DropGaussian [46] and our DropAnSH-GS.** (a) DropGaussian randomly sets the opacity of individual Gaussians to zero. (b) DropAnSH-GS selects random Gaussians as anchors, discards their neighbors, and applies Dropout to high-degree SH. Anchor-based Dropout eliminates contiguous 3D regions, which effectively inhibits adjacent Gaussians from compensating for the dropped ones, forcing remaining Gaussians to learn more robust scene representations, thereby strengthening the Dropout regularization effect. Dropping SH further reduces overfitting and yields a more compact model.

distortions that limit its practical applicability.

Inspired by regularization techniques in deep learning [52], recent works introduce the Dropout mechanism into 3DGS [46, 58]. These methods randomly set the opacity of certain Gaussians to zero during training, aiming to prevent over-reliance on specific Gaussians and thereby regularize the model. However, our analysis reveals critical limitations in these approaches: (1) *Neighbor compensation effect* (Figure 2). 3DGS leverages numerous overlapping Gaussians to collaboratively render a scene, which often exhibits highly similar opacity and color attributes in local regions. When a single Gaussian is dropped, its rendering contribution is easily compensated by neighboring

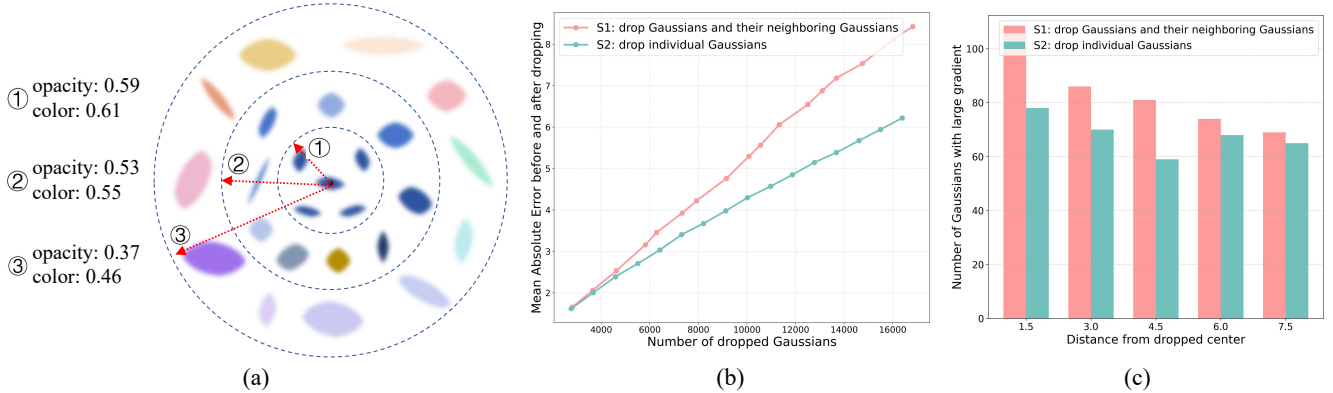


Figure 2. **Compensation effect in neighbor Gaussians.** (a) We measure the spatial autocorrelation of opacity and color between Gaussians at varying distances using Moran’s I metric [37, 40]. Closer Gaussians exhibit higher similarity in opacity and color. This spatial redundancy implies that dropping only individual Gaussians can be easily compensated for by their surrounding similar neighbors, thereby limiting the effectiveness of dropout. (b) We report the Mean Absolute Error between rendered images before and after applying two different Dropout strategies, S1 and S2. When dropping a similar number of Gaussians, the strategy that drops Gaussians and their neighboring Gaussians (S1) has a larger impact on rendering quality, as it avoids simple compensation by neighboring Gaussians. (c) In regions surrounding the dropped Gaussians, the S1 strategy activates a greater number of remaining Gaussians, resulting in stronger gradient updates.

ones, thereby weakening the intended regularization effect of Dropout. (2) *Limited attribute utilization* (Figure 3). Existing dropout strategies in 3DGS exclusively target the opacity attribute, while neglecting the distinct roles of other attributes in overfitting.

To address these limitations, we propose a novel Dropout regularization strategy termed DropAnSH-GS. Unlike previous Dropout strategies [46, 58] that discard isolated Gaussians, DropAnSH-GS randomly selects a set of anchor Gaussians and drops these anchors and their surrounding neighbours within a local spatial region. This structured Dropout strategy eliminates entire clusters of correlated Gaussians, creating larger-scale “information voids” that actively disrupt spatial coherence and prevent local compensation. Consequently, the optimization process is compelled to utilize more long-range contextual information to reconstruct the dropped regions, thereby fostering more robust and generalizable scene representations.

Moreover, existing 3DGS Dropout methods are limited to manipulating opacity without considering the nuanced differences among multiple attributes. We identify that SH, particularly higher-degree terms, also cause overfitting (as shown in Figure 3). To this end, we further introduce a Dropout mechanism targeting high-degree SH. This strategy provides twofold benefits: it (1) mitigates overfitting to color variations, and (2) promotes a coarse-to-fine SH representation, prioritizing lower-degree SH for scene representation. Consequently, the trained model permits post-hoc pruning of high-degree SH to obtain a more compact model without requiring retraining, as shown in Figure 1.

The main contributions of our work are as follows:

- We identify and analyze the limitations of existing

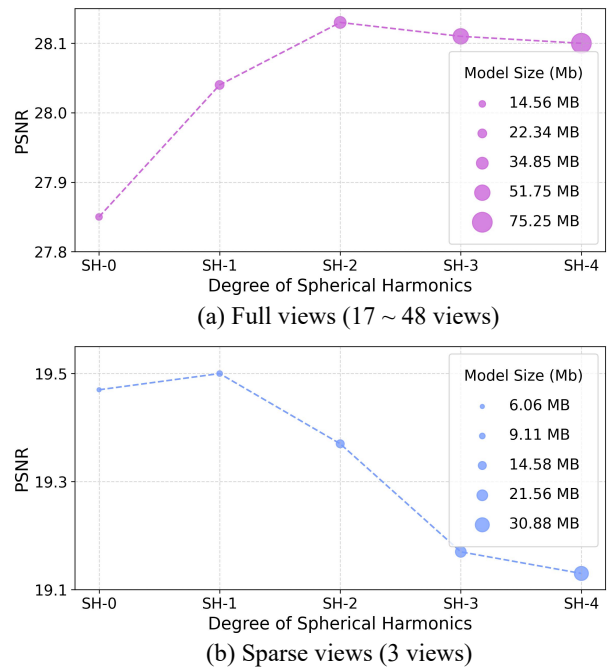


Figure 3. **Overfitting caused by high-degree SH.** On the LLFF dataset, (a) under full-view conditions, moderately increasing the degree of spherical harmonics can improve the performance of the 3DGS model. However, (b) under sparse-view settings, using high-degree spherical harmonics leads to performance degradation and a significant increase in model size, indicating that spherical harmonics themselves also constitute a source of overfitting.

Dropout strategies in 3DGS, showcasing how spatial redundancy and high-degree spherical harmonic coeffi-

cients weaken their regularization effect.

- We propose DropAnSH-GS, a novel structured spatial Dropout method that discards clusters of Gaussians, achieving stronger regularization against overfitting.
- We extend the Dropout strategy to appearance attributes by dropping SH, which simultaneously suppresses overfitting and enables flexible post-hoc model compression.
- Comprehensive experiments demonstrate that our method significantly outperforms the state-of-the-art Dropout techniques for 3DGS, while incurring negligible additional computational cost. Moreover, it can be used to enhance the quality of multiple 3DGS variants, highlighting its broad applicability and value.

2. Related Work

NeRF and 3DGS. Neural Radiance Fields (NeRF) implicitly model 3D scenes using neural networks to enable high-quality novel view synthesis [1, 3, 29, 35, 36, 39, 41, 42, 45, 47, 48, 53, 62]. However, the training and rendering processes of NeRF are computationally intensive, limiting its applicability in real-time scenarios [10, 11, 18, 26, 33, 49, 50, 55, 57]. Subsequent efforts, such as Instant-NGP [41] and Plenoxels [15], improve efficiency through network architecture optimization or by introducing explicit scene representations. Recently, 3DGS has gained significant attention as an efficient explicit representation [17, 21, 23–25, 31, 32, 37, 59]. It models the 3D scene as a set of Gaussian functions, using attributes such as position, covariance, opacity, and spherical harmonic coefficients for fast and high-fidelity rendering. Follow-up works have further enhanced 3DGS in terms of parameter efficiency and rendering quality [2, 5–8, 14, 21, 27, 30–32, 44, 61].

NVS under Sparse Views. Novel view synthesis under sparse views aims to generate high-quality novel views from limited input images. Prior studies [4, 16, 22, 37, 43, 54, 60] have noted that the performance of both NeRF and 3DGS methods heavily depends on the dense views. To address this, researchers have proposed various methods to enhance NeRF’s generalization under sparse views, such as DietNeRF [22], RegNeRF [43], and FreeNeRF [60], which employ diverse regularization loss strategies to mitigate overfitting. For sparse-view optimization in 3DGS, FSGS [66] introduces a Proximity-guided Gaussian Unpooling strategy, CoR-GS [63] uses mutual constraints between two distinct 3DGS models, InstantSplat [9] jointly optimizes poses, while DNGaussian [28] and NexusGS [65] introduce the depth constraint to enhance the performance of the 3DGS model.

Dropout Technique in 3DGS. In this work, we focus on leveraging the Dropout technique to improve the performance of 3DGS under sparse-view conditions. The most closely related works are DropoutGS [58] and DropGaus-

sian [46], both of which propose mitigating overfitting in 3DGS by randomly discarding Gaussians during training. However, the high correlation among neighboring Gaussians limits the effectiveness of their Dropout strategies. In contrast, our DropAnSH-GS method significantly strengthens regularization by discarding clusters of neighboring Gaussians and applying Dropout to spherical harmonic coefficients. Our approach achieves a flexible trade-off between performance and model size, offering a novel solution for the sparse-view NVS task.

3. Method

3.1. Preliminaries

3DGS represents a 3D scene using a large number of explicit Gaussians. Each Gaussian G_i is parameterized by: position $\mu_i \in \mathbb{R}^3$, covariance $\Sigma_i \in \mathbb{R}^{3 \times 3}$, color c_i (represented by a set of spherical harmonics coefficients), and opacity $\alpha_i \in [0, 1]$. For efficient optimization, the covariance Σ_i is typically factorized into a scaling vector $s_i \in \mathbb{R}^3$ and a rotation quaternion $q_i \in \mathbb{R}^4$. Given a camera view defined by a view matrix W , the 3D Gaussians are projected onto the 2D image plane. The color C of a pixel is computed using α -blending over all N depth-sorted Gaussians:

$$C = \sum_{i=1}^N c_i \alpha_i \prod_{j=1}^{i-1} (1 - \alpha_j). \quad (1)$$

3.2. Pilot Study

To mitigate overfitting under sparse view settings, prior works propose randomly setting the opacity α_i of Gaussians to zero during training. However, the expressive nature of 3DGS exhibits significant local redundancy. A visible surface is typically represented by hundreds or thousands of overlapping Gaussians. When a single Gaussian is removed, as per Eq. (1), its contribution to pixel color is compensated by the increased contributions of neighboring Gaussians. Consequently, the change in pixel color ΔC is negligible, resulting in weak gradient signals during back-propagation that fail to impose effective regularization on the model’s geometry and appearance learning.

As illustrated in Figure 2, spatial correlation among Gaussians is inversely related to their distance. Removing a single Gaussian within the view frustum results in minimal performance degradation and weak gradients. In contrast, discarding a cluster of 10 neighboring Gaussians produces significant performance changes and stronger gradient signals. This suggests that Gaussians exhibit strong spatial complementarity. While this facilitates cooperative rendering, it also diminishes the effectiveness of naive Dropout.

Moreover, existing methods focus solely on dropping opacity values, overlooking the regularization potential of

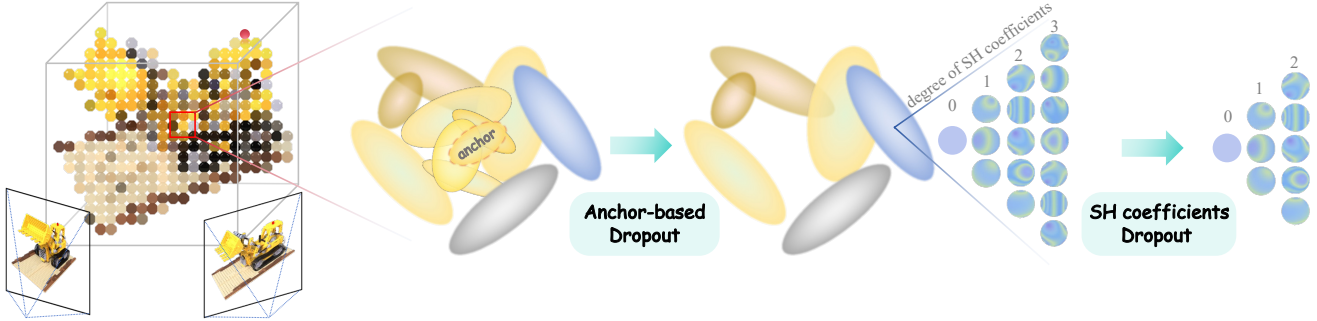


Figure 4. **Overview of DropAnSH-GS.** During the training phase, we randomly select a set of anchor Gaussians and drop these anchors and their surrounding neighbours within a local spatial region, thereby reducing the likelihood of neighboring Gaussians compensating for one another and enhancing the regularization effect. Simultaneously, high-degree SH coefficients are randomly dropped to further strengthen regularization and yield a more compact model representation.

other crucial attributes, such as the spherical harmonic coefficients that encode appearance. As illustrated in Figure 3, while using high-degree SH improves performance under full-view conditions, it leads to overfitting in sparse-view settings. Appropriately reducing the degree of SH not only enhances 3DGS performance in sparse-view scenarios but also significantly reduces the model size.

3.3. Anchor-based Dropout

To overcome the above limitations, we propose DropAnSH-GS method, as illustrated in Figure 4, which drops groups of spatially related Gaussians rather than individual, isolated ones. The core idea is to remove entire regions of information, thereby forcing the model to rely on broader contextual cues for reconstruction and encouraging the learning of non-local, structural scene features. This process is executed during training with the following steps:

1. *Anchor Selection:* We randomly select a subset of anchor Gaussians $\mathcal{A} \subset \mathcal{G}$ from the set of all N Gaussians $\mathcal{G} = \{G_1, \dots, G_N\}$, based on a sampling ratio p_a .
2. *Neighborhood Construction:* For each anchor Gaussian in \mathcal{A} , we identify its k nearest neighboring Gaussians in Euclidean space based on the distance between their centers.
3. *Structured Dropout:* All Gaussians that belong to any anchor or its neighborhood are collected into a Dropout set \mathcal{D} . We then define a binary mask vector $M \in \{0, 1\}^N$ for all Gaussians. For each G_i , its mask value m_i is:

$$m_i = \begin{cases} 0 & \text{if } G_i \in \mathcal{D} \\ 1 & \text{otherwise} \end{cases}. \quad (2)$$

During training, the original opacity α_i of each Gaussian is modulated by its mask to obtain the effective opacity $\hat{\alpha}_i$:

$$\hat{\alpha}_i = \alpha_i \cdot m_i. \quad (3)$$

This modulated opacity $\hat{\alpha}_i$ is then used in the α -blending process in Eq. (1), effectively creating “information voids” in the 3D scene and enforcing stronger regularization.

3.4. Spherical Harmonics Dropout

Existing Dropout methods focus solely on the presence or absence of Gaussians according to opacity, overlooking the distinct characteristics of other attributes in Dropout. We observe that high-degree SH coefficients are also prone to overfitting. To address this, we propose a Dropout strategy targeting these coefficients. Specifically, the color \mathbf{c} of a Gaussian is represented by SH coefficients up to degree L :

$$\mathbf{c} = [\mathbf{c}^{(0)}, \mathbf{c}^{(1)}, \dots, \mathbf{c}^{(L)}], \quad (4)$$

where $\mathbf{c}^{(l)}$ denotes the SH coefficients of degree l , comprising $2l + 1$ values per RGB channel. During training, we randomly select a subset of Gaussians with probability p_{sh} and set a maximum retained degree l_{\max} , then discard all SH coefficients of degree higher than l_{\max} .

$$\tilde{\mathbf{c}} = [\mathbf{c}^{(0)}, \dots, \mathbf{c}^{(l_{\max})}, \mathbf{0}, \dots, \mathbf{0}]. \quad (5)$$

This Dropout forces the model to prioritize low-degree SH coefficients for basic appearance. As training progresses, l_{\max} gradually increases to allow more high-frequency detail. After training, higher-degree coefficients become optional, allowing users to discard them to obtain a smaller and faster model without retraining. This enables flexible trade-offs between performance and efficiency.

3.5. Loss Function

Our proposed strategies can be seamlessly integrated into the training pipeline of existing 3DGS frameworks without modifying their objective functions. We adopt the standard loss that minimizes the difference between the rendered image \hat{C} and the ground truth C_{gt} using a combination of L1 Norm and SSIM losses [25]:

$$\mathcal{L} = \mathcal{L}_{L1}(\hat{C}, C_{gt}) + \lambda \mathcal{L}_{SSIM}(\hat{C}, C_{gt}), \quad (6)$$

where λ is a balancing weight that controls the relative contribution of the L1 and SSIM terms.

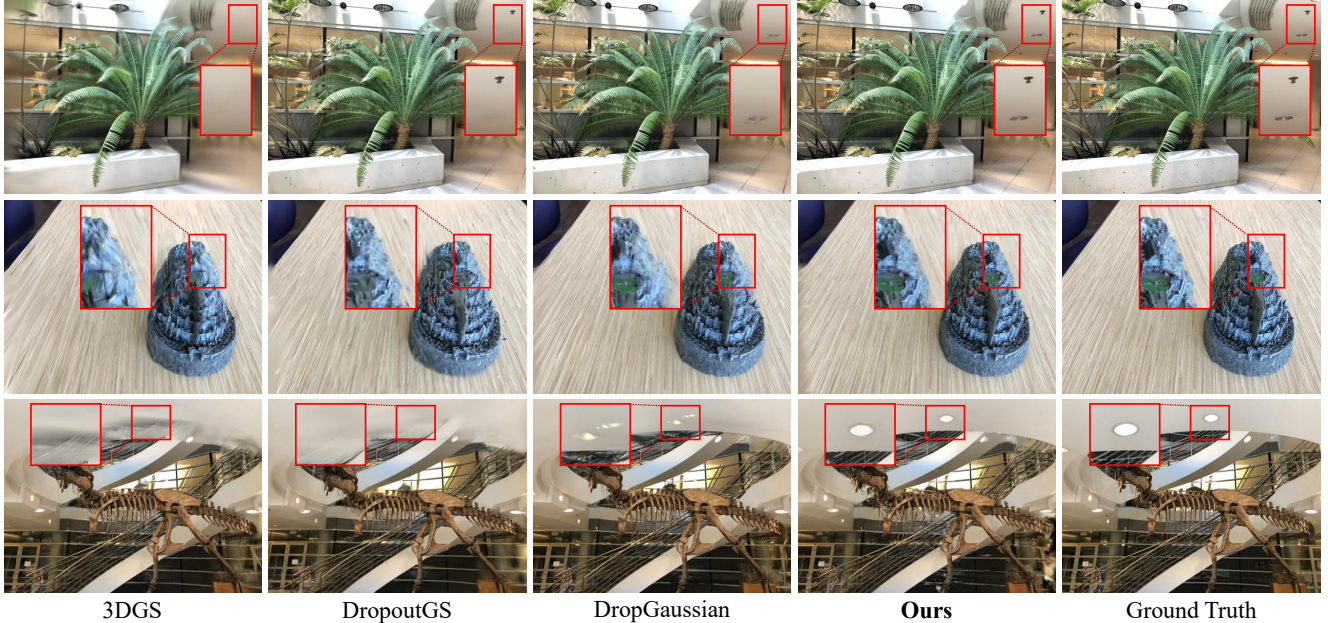


Figure 5. Qualitative comparison on the LLFF dataset (3 views).

Table 1. Quantitative comparison on the LLFF dataset (3, 6 and 9 views).

	Methods	3-view			6-view			9-view		
		PSNR \uparrow	SSIM \uparrow	LPIPS \downarrow	PSNR \uparrow	SSIM \uparrow	LPIPS \downarrow	PSNR \uparrow	SSIM \uparrow	LPIPS \downarrow
NeRF-based	Mip-NeRF [4]	16.11	0.401	0.460	22.91	0.756	0.213	24.88	0.826	0.170
	DietNeRF [22]	14.94	0.370	0.496	21.75	0.717	0.248	24.28	0.801	0.183
	RegNeRF [43]	19.08	0.587	0.336	23.10	0.760	0.206	24.86	0.820	0.161
	FreeNeRF [60]	19.63	0.612	0.308	23.73	0.779	0.195	25.13	0.827	0.160
3DGS-based	3DGS [25]	19.17	0.646	0.268	23.74	0.807	0.162	25.44	0.860	0.096
	DNGaussian [28]	19.12	0.591	0.294	22.18	0.755	0.198	23.17	0.788	0.180
	FSGS [66]	20.43	0.682	0.248	24.09	0.823	0.145	25.31	0.860	0.122
	CoR-GS [63]	<u>20.36</u>	<u>0.710</u>	0.202	24.34	<u>0.831</u>	<u>0.122</u>	25.94	<u>0.872</u>	0.088
	DropoutGS [58]	19.39	0.632	0.279	24.02	0.816	0.144	25.13	0.869	0.099
	DropGaussian [46]	20.33	0.709	<u>0.201</u>	<u>24.58</u>	0.830	0.125	25.85	0.864	<u>0.093</u>
	Ours	20.68	0.724	0.194	24.76	0.837	0.116	26.24	0.875	0.088

4. Experiments

4.1. Implementation Details

Datasets. Our experiments are conducted on three standard datasets: two real-world datasets of LLFF [38] and MipNeRF-360 [4], and one synthetic dataset of Blender [39]. We follow previous works [46, 54, 60] to split the datasets into training and testing subsets with varying numbers of input views.

Metrics. To comprehensively evaluate rendering quality, we adopt three widely used metrics: Peak Signal-to-Noise Ratio (PSNR, higher is better), Structural Similarity Index [56] (SSIM, higher is better), and Learned Perceptual

Image Patch Similarity [64] (LPIPS, lower is better).

Baselines. We compare our method against several state-of-the-art approaches, including NeRF-based sparse-view methods (Mip-NeRF [4], RegNeRF [43], DietNeRF [22], FreeNeRF [60]) and 3DGS-based methods (3DGS [25], DNGaussian [28], FSGS [66], CoR-GS [63]). We particularly focus on comparing with two Dropout-based methods, DropGaussian [46] and DropoutGS [58].

Training Details. All experiments are implemented using the PyTorch framework and conducted on a single NVIDIA H100 GPU. We maintain the same optimizer settings and learning rate strategy as the original 3DGS, training for 10,000 iterations across all datasets. The key hyperparam-

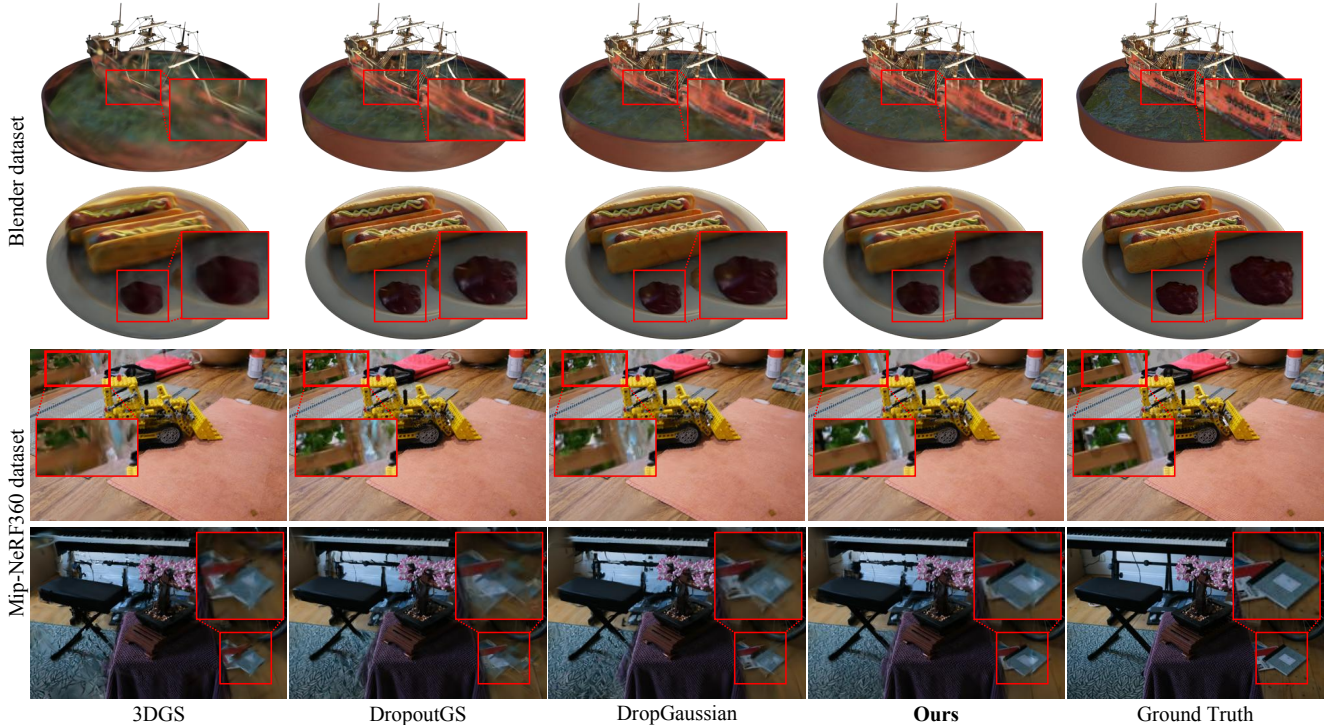


Figure 6. Qualitative comparisons on the Blender (8 views) and MipNeRF-360 (12 views) datasets.

Table 2. Quantitative comparison on the MipNeRF-360 (12 views) and Blender (8 views) datasets. SH_n denotes retaining only the first n degrees of SH coefficients during inference.

Methods	MipNeRF-360		Blender	
	PSNR \uparrow	Size (Mb) \downarrow	PSNR \uparrow	Size (Mb) \downarrow
3DGS [25]	18.58	143.4	22.13	6.5
DNGaussian [28]	18.84	80.7	24.31	5.5
FSGS [66]	18.80	172.1	24.64	8.4
CoR-GS [63]	19.42	117.4	24.31	6.3
DropoutGS [58]	19.17	68.4	24.79	5.2
DropGaussian [46]	19.66	120.7	25.17	6.0
Ours- SH_0	19.71	33.8	25.04	1.7
Ours- SH_1	19.86	<u>51.8</u>	25.34	<u>2.6</u>
Ours- SH_2	19.95	81.1	<u>25.47</u>	4.1
Ours- SH_3	<u>19.93</u>	122.6	25.50	6.2

ters are set as follows: the anchor sampling rate p_a linearly increases from 0 to 0.02 based on the value of iterations; The number of nearest neighboring Gaussians k is set to 10; the Dropout rate for SH coefficients p_{sh} is 0.2, with l_{max} set to 0, 1, and 2 at 2,000, 4,000, and 6,000 iterations, respectively. For methods involving randomness, including ours, CoR-GS, and the Dropout-based baselines, we report the mean metrics over 3 independent runs.

For more experimental results, please refer to the supplementary materials.

4.2. Comparison Results

Quantitative Comparison. We first perform quantitative evaluations on the LLFF, MipNeRF-360 and Blender datasets under varying sparse view conditions, with results presented in Tables 1 and 2. Our method consistently outperforms all baselines. On the LLFF dataset, particularly in the extremely sparse 3-view setting, our method significantly surpasses other Dropout-based approaches that discard individual Gaussians. This demonstrates the effectiveness of the proposed anchor-based Dropout strategy. As the number of views increases, our approach continues to significantly enhance 3DGS performance. Similar performance is observed on the MipNeRF-360 and Blender datasets, confirming that our regularization technique robustly addresses the core challenges of 3DGS under sparse-view conditions.

Qualitative Comparison. As illustrated in Figures 5 and 6, we provide qualitative comparisons across various scenes, illustrating the superiority of our method. By removing entire regions, our method simulates occlusions and missing information, prompting Gaussians to store more complete scene context. This leads to more complete and consistent novel view synthesis, as evidenced in Figure 5, where our method preserves more structural detail compared to baselines, which suffer from distortion artifacts and information loss. Furthermore, baseline methods produce numer-

Figure 7. **Compatibility to different 3DGS variants on the LLFF dataset (3 views)**. The proposed DropAnSH-GS can be easily integrated into other 3DGS-based methods and improve their performance.

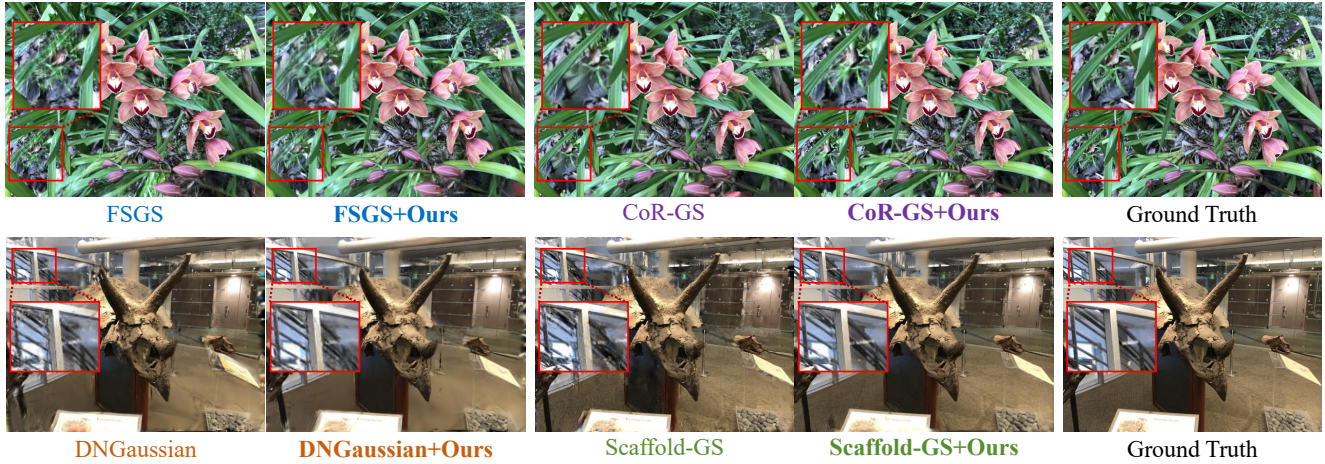


Table 3. **Compatibility to 3DGS variants on the LLFF dataset (3 views)**. The proposed DropAnSH-GS can be easily integrated into various 3DGS-based methods and improve their performance.

Methods	PSNR \uparrow	SSIM \uparrow	LPIPS \downarrow
FSGS [66]	20.43	0.682	0.248
FSGS+Ours	20.72	0.713	0.205
CoR-GS [63]	20.36	0.710	0.202
CoR-GS+Ours	20.74	0.718	0.203
DNGaussian [28]	19.12	0.591	0.294
DNGaussian+Ours	19.71	0.639	0.268
Scaffold-GS [31]	18.62	0.643	0.258
Scaffold-GS+Ours	19.84	0.679	0.212

ous Gaussian-shaped artifacts in Figure 6, especially around object boundaries and in the background. In contrast, our method effectively suppresses these issues by discouraging the model from overfitting complex surfaces with a small number of high-opacity Gaussians, resulting in smoother and more natural geometric structures.

4.3. Compression of Model Size

A unique aspect of our method is the Dropout of SH coefficients, which enables the scene appearance to be stored incrementally from low-degree to high-degree terms. At inference time, the trained model can be truncated by removing high-degree SH coefficients. As shown in Tables 2, even a model retaining only the zeroth-degree SH coefficients outperforms the vanilla 3DGS, while requiring only 25% of the parameters. This provides a flexible way to balance model size and performance.

Table 4. **Comparison of training time on different datasets**. We achieve a substantial performance improvement with a negligible increase in computational time.

Method	PSNR \uparrow	SSIM \uparrow	LPIPS \downarrow	Total Time \downarrow
LLFF dataset (3 views)				
3DGS	19.17	0.646	0.268	741.6s
Ours	20.68	0.724	0.194	760.2s
Blender dataset (8 views)				
3DGS	22.13	0.855	0.132	863.3s
Ours	25.50	0.891	0.088	887.7s
MipNeRF-360 dataset (12 views)				
3DGS	18.58	0.526	0.419	1083.2s
Ours	19.93	0.576	0.362	1114.8s

4.4. Compatibility

The proposed Dropout framework is lightweight and modular, making it easy to plug into other 3DGS variants. As shown in Table 3 and Figure 7, applying our framework to the FSGS [66], Cor-GS [63], DNGaussian [28], and Scaffold-GS [31] significantly improves their performance under sparse view conditions. This suggests that our method is broadly applicable and can enhance the robustness of other 3DGS frameworks in view-scarce scenarios.

4.5. Training Efficiency

Our method introduces an additional computational step during training, i.e., nearest neighbor search for anchor Gaussians. To accelerate this process, we implement it efficiently using CUDA on GPUs [19]. We run our method and the vanilla 3DGS on the same NVIDIA H100 GPU for 10,000 iterations to compare their total training time

Table 5. **Hyperparameter sensitivity of the anchor selection probability p_a , number of neighbors k , and SH Dropout probability p_{sh} .** The evaluation is conducted on the LLFF dataset (3 views).

p_a	PSNR \uparrow	SSIM \uparrow	LPIPS \downarrow	k	PSNR \uparrow	SSIM \uparrow	LPIPS \downarrow	p_{sh}	PSNR \uparrow	SSIM \uparrow	LPIPS \downarrow
0.005	20.25	0.705	0.211	1	20.12	0.701	0.216	0.1	20.56	0.721	0.198
0.01	20.50	0.718	0.194	5	20.39	0.719	0.200	0.2	20.68	0.724	0.194
0.02	20.68	0.724	0.194	10	20.68	0.724	0.194	0.3	20.65	0.725	0.197
0.03	20.32	0.710	0.202	15	20.43	0.721	0.198	0.4	20.44	0.713	0.202
0.04	19.97	0.665	0.257	20	20.07	0.706	0.224	0.5	20.49	0.711	0.208

Table 6. **Ablation results of the designed components on the LLFF datasets (3 views).**

Settings		PSNR \uparrow	SSIM \uparrow	LPIPS \downarrow
Drop Anchor	Drop SH			
×	×	19.17	0.646	0.268
✓	×	20.47	0.713	0.200
×	✓	19.59	0.641	0.247
✓	✓	20.68	0.724	0.194

Table 7. **Ablation results of different SH Dropout strategies on the Blender dataset (8 views).**

	PSNR \uparrow	SSIM \uparrow	LPIPS \downarrow
Drop SH Randomly	25.12	0.885	0.097
Drop SH by Degree (Ours)	25.50	0.891	0.088

on different datasets. As shown in Table 4, our method incurs only a modest increase in training time (less than 2.8% compared to 3DGS). Given the substantial improvement in rendering quality (an average PSNR gain of 2 dB), this marginal computational cost is well justified.

4.6. Ablation Study

Effectiveness of each dropout component. We conduct ablation studies in Table 6, revealing the following: (1) Removing the “Drop Anchor” strategy leads to significant performance declines across all metrics, confirming the efficacy of our spatial Anchor-based Dropout in breaking local redundancy for regularization. (2) Omitting the “Drop SH” module also results in performance degradation, demonstrating that regularizing appearance attributes is another effective approach to mitigating overfitting. The full model achieves the best performance, indicating that Drop Anchor and Drop SH are complementary and jointly enhance the model’s overall performance.

Drop SH by Degree vs Drop SH Randomly. In DropAnSH-GS, we use a “Drop SH by Degree” strategy for discarding high-degree SH coefficients during training. We compare it against a more direct baseline: “Drop SH Randomly”. In this alternative strategy, we do not operate on entire degrees but instead randomly set individual SH co-

efficients to zero with the same probability. The results in Table 7 demonstrate that our “Drop SH by Degree” strategy significantly outperforms randomly dropping individual SH coefficients.

Hyperparameter Sensitivity Analysis. We conduct a sensitivity analysis on three key hyperparameters: (1) anchor selection probability p_a (default: 0.02), (2) number of neighbors k (default: 10), and (3) SH Dropout probability p_{sh} (default: 0.2). Experiments are performed on the LLFF dataset (3 views), with results in Table 5. The parameter p_a controls the proportion of Gaussians selected as anchors. A small p_a gives insufficient regularization. Conversely, an excessively large p_a drops too many Gaussians, which can disrupt the scene’s geometric structure and degrade performance. The Number of Neighbors k determines the size of the “information voids” around each anchor. A small k creates voids that are too small and easily compensated for, weakening the regularization effect; too large k removes critical local structures and hurts performance. The probability p_{sh} controls the dropout of high-degree SH coefficients to prevent overfitting to fine color details. A lower value of p_{sh} provides insufficient regularization, while a higher value overly penalizes the SH coefficients, degrading performance.

5. Conclusions

In this work, we address the severe overfitting issue of 3DGS under sparse views. We are the first to identify that the existing methods based on independent random Dropout stem from the spatial redundancy of Gaussians, which enables local compensation effects to undermine the regularization strength. We further observe that high-degree spherical harmonic coefficients contribute to overfitting in 3DGS. To this end, we propose DropAnSH-GS, a novel Dropout strategy that discards entire spatial regions rather than isolated Gaussians and effectively disrupts local information dependencies, compelling the model to learn more robust global scene representations. Furthermore, we extend Dropout to appearance attributes to reduce overfitting and enable post-training scalability. Our method is simple yet effective, significantly enhancing the 3DGS and its variants under limited-view conditions.

References

- [1] Matan Atzmon, Niv Haim, Lior Yariv, Ofer Israelov, Haggai Maron, and Yaron Lipman. Controlling neural level sets. *Advances in Neural Information Processing Systems*, 2019. 3
- [2] Milena T Bagdasarian, Paul Knoll, Florian Barthel, Anna Hilsmann, Peter Eisert, and Wieland Morgenstern. 3dgs. zip: A survey on 3d gaussian splatting compression methods. *arXiv preprint arXiv:2407.09510*, 2024. 1, 3
- [3] Jonathan T Barron, Ben Mildenhall, Matthew Tancik, Peter Hedman, Ricardo Martin-Brualla, and Pratul P Srinivasan. Mip-nerf: A multiscale representation for anti-aliasing neural radiance fields. In *Proceedings of the IEEE/CVF international conference on computer vision*, pages 5855–5864, 2021. 3
- [4] Jonathan T Barron, Ben Mildenhall, Dor Verbin, Pratul P Srinivasan, and Peter Hedman. Mip-nerf 360: Unbounded anti-aliased neural radiance fields. In *Proceedings of the IEEE/CVF conference on computer vision and pattern recognition*, pages 5470–5479, 2022. 3, 5
- [5] Guikun Chen and Wenguan Wang. A survey on 3d gaussian splatting. *arXiv preprint arXiv:2401.03890*, 2024. 1, 3
- [6] Yihang Chen, Qianyi Wu, Weiyao Lin, Mehrtash Harandi, and Jianfei Cai. Hac: Hash-grid assisted context for 3d gaussian splatting compression. In *European Conference on Computer Vision*, pages 422–438. Springer, 2025. 1
- [7] Yuedong Chen, Haofei Xu, Chuanxia Zheng, Bohan Zhuang, Marc Pollefeys, Andreas Geiger, Tat-Jen Cham, and Jianfei Cai. Mvsplat: Efficient 3d gaussian splatting from sparse multi-view images. In *European Conference on Computer Vision*, pages 370–386. Springer, 2025.
- [8] Devikalyan Das, Christopher Wewer, Raza Yunus, Eddy Ilg, and Jan Eric Lenssen. Neural parametric gaussians for monocular non-rigid object reconstruction. In *Proceedings of the IEEE/CVF Conference on Computer Vision and Pattern Recognition*, pages 10715–10725, 2024. 3
- [9] Zhiwen Fan, Wenyan Cong, Kairun Wen, Kevin Wang, Jian Zhang, Xinghao Ding, Danfei Xu, Boris Ivanovic, Marco Pavone, Georgios Pavlakos, et al. Instantsplat: Unbounded sparse-view pose-free gaussian splatting in 40 seconds. *arXiv preprint arXiv:2403.20309*, 2, 2024. 1, 3
- [10] Shuangkang Fang, Yufeng Wang, Yi Yang, Yi-Hsuan Tsai, Wenrui Ding, Shuchang Zhou, and Ming-Hsuan Yang. Editing 3d scenes via text prompts without retraining. *arXiv e-prints*, pages arXiv–2309, 2023. 3
- [11] Shuangkang Fang, Weixin Xu, Heng Wang, Yi Yang, Yufeng Wang, and Shuchang Zhou. One is all: Bridging the gap between neural radiance fields architectures with progressive volume distillation. In *Proceedings of the AAAI Conference on Artificial Intelligence*, pages 597–605, 2023. 3
- [12] Shuangkang Fang, Yufeng Wang, Yi-Hsuan Tsai, Yi Yang, Wenrui Ding, Shuchang Zhou, and Ming-Hsuan Yang. Chat-edit-3d: Interactive 3d scene editing via text prompts. *arXiv preprint arXiv:2407.06842*, 2024. 1
- [13] Shuangkang Fang, I Shen, Takeo Igarashi, Yufeng Wang, ZeSheng Wang, Yi Yang, Wenrui Ding, Shuchang Zhou, et al. Nerf is a valuable assistant for 3d gaussian splatting. In *Proceedings of the IEEE/CVF International Conference on Computer Vision*, pages 26230–26240, 2025. 1
- [14] Yalda Foroutan, Daniel Rebain, Kwang Moo Yi, and Andrea Tagliasacchi. Does gaussian splatting need sfm initialization? *arXiv preprint arXiv:2404.12547*, 2024. 3
- [15] Sara Fridovich-Keil, Alex Yu, Matthew Tancik, Qinhong Chen, Benjamin Recht, and Angjoo Kanazawa. Plenoxels: Radiance fields without neural networks. In *Proceedings of the IEEE/CVF conference on computer vision and pattern recognition*, pages 5501–5510, 2022. 3
- [16] Yang Fu, Sifei Liu, Amey Kulkarni, Jan Kautz, Alexei A. Efros, and Xiaolong Wang. Colmap-free 3d gaussian splatting. In *Proceedings of the IEEE/CVF Conference on Computer Vision and Pattern Recognition*, pages 20796–20805, 2024. 1, 3
- [17] Jian Gao, Chun Gu, Youtian Lin, Hao Zhu, Xun Cao, Li Zhang, and Yao Yao. Relightable 3d gaussian: Real-time point cloud relighting with brdf decomposition and ray tracing. *arXiv preprint arXiv:2311.16043*, 2023. 3
- [18] Stephan J Garbin, Marek Kowalski, Matthew Johnson, Jamie Shotton, and Julien Valentin. Fastnerf: High-fidelity neural rendering at 200fps. In *Proceedings of the IEEE/CVF international conference on computer vision*, pages 14346–14355, 2021. 3
- [19] Vincent Garcia, Éric Debreuve, Frank Nielsen, and Michel Barlaud. k-nearest neighbor search: fast gpu-based implementations and application to high-dimensional feature matching. In *Proceedings of the IEEE International Conference on Image Processing*, pages 3757–3760, 2010. 7
- [20] Liang Han, Junsheng Zhou, Yu-Shen Liu, and Zhizhong Han. Binocular-guided 3d gaussian splatting with view consistency for sparse view synthesis. *Advances in Neural Information Processing Systems*, 37:68595–68621, 2024. 1
- [21] Binbin Huang, Zehao Yu, Anpei Chen, Andreas Geiger, and Shenghua Gao. 2d gaussian splatting for geometrically accurate radiance fields. *arXiv preprint arXiv:2403.17888*, 2024. 1, 3
- [22] Ajay Jain, Matthew Tancik, and Pieter Abbeel. Putting nerf on a diet: Semantically consistent few-shot view synthesis. In *Proceedings of the IEEE/CVF International Conference on Computer Vision*, pages 5885–5894, 2021. 3, 5
- [23] Yingwenqi Jiang, Jiadong Tu, Yuan Liu, Xifeng Gao, Xiaoxiao Long, Wenping Wang, and Yuexin Ma. Gaussian-shader: 3d gaussian splatting with shading functions for reflective surfaces. In *Proceedings of the IEEE/CVF Conference on Computer Vision and Pattern Recognition*, pages 5322–5332, 2024. 1, 3
- [24] Jaewoo Jung, Jisang Han, Honggyu An, Jiwon Kang, Seonghoon Park, and Seungryong Kim. Relaxing accurate initialization constraint for 3d gaussian splatting. *arXiv preprint arXiv:2403.09413*, 2024.
- [25] Bernhard Kerbl, Georgios Kopanas, Thomas Leimkühler, and George Drettakis. 3d gaussian splatting for real-time radiance field rendering. *ACM Transactions on Graphics*, 42(4):1–14, 2023. 1, 3, 4, 5, 6
- [26] Byeonghyeon Lee, Howoong Lee, Usman Ali, and Eunbyung Park. Sharp-nerf: Grid-based fast deblurring neural

- radiance fields using sharpness prior. In *Proceedings of the IEEE/CVF Winter Conference on Applications of Computer Vision*, pages 3709–3718, 2024. 3
- [27] Joo Chan Lee, Daniel Rho, Xiangyu Sun, Jong Hwan Ko, and Eunbyung Park. Compact 3d gaussian representation for radiance field. In *Proceedings of the IEEE/CVF Conference on Computer Vision and Pattern Recognition*, pages 21719–21728, 2024. 3
- [28] Jiahe Li, Jiawei Zhang, Xiao Bai, Jin Zheng, Xin Ning, Jun Zhou, and Lin Gu. Dngaussian: Optimizing sparse-view 3d gaussian radiance fields with global-local depth normalization. In *Proceedings of the IEEE/CVF conference on computer vision and pattern recognition*, pages 20775–20785, 2024. 3, 5, 6, 7
- [29] David B Lindell, Julien NP Martel, and Gordon Wetzstein. Autoint: Automatic integration for fast neural volume rendering. In *Proceedings of the IEEE/CVF Conference on Computer Vision and Pattern Recognition*, pages 14556–14565, 2021. 3
- [30] Xiangrui Liu, Xinju Wu, Pingping Zhang, Shiqi Wang, Zhu Li, and Sam Kwong. Compgs: Efficient 3d scene representation via compressed gaussian splatting. *arXiv preprint arXiv:2404.09458*, 2024. 1, 3
- [31] Tao Lu, Mulin Yu, Linning Xu, Yuanbo Xiangli, Limin Wang, Dahua Lin, and Bo Dai. Scaffold-gs: Structured 3d gaussians for view-adaptive rendering. In *Proceedings of the IEEE/CVF Conference on Computer Vision and Pattern Recognition*, pages 20654–20664, 2024. 1, 3, 7
- [32] Dawid Malarz, Weronika Smolak, Jacek Tabor, Sławomir Tadeja, and Przemysław Spurek. Gaussian splatting with nerf-based color and opacity. *arXiv preprint arXiv:2312.13729*, 2023. 3
- [33] Ricardo Martin-Brualla, Noha Radwan, Mehdi SM Sajjadi, Jonathan T Barron, Alexey Dosovitskiy, and Daniel Duckworth. Nerf in the wild: Neural radiance fields for unconstrained photo collections. In *Proceedings of the IEEE/CVF conference on computer vision and pattern recognition*, pages 7210–7219, 2021. 3
- [34] Hidenobu Matsuki, Riku Murai, Paul HJ Kelly, and Andrew J Davison. Gaussian splatting slam. In *Proceedings of the IEEE/CVF Conference on Computer Vision and Pattern Recognition*, pages 18039–18048, 2024. 1
- [35] Lars Mescheder, Michael Oechsle, Michael Niemeyer, Sebastian Nowozin, and Andreas Geiger. Occupancy networks: Learning 3d reconstruction in function space. In *Proceedings of the IEEE/CVF Conference on Computer Vision and Pattern Recognition*, pages 4460–4470, 2019. 3
- [36] Mateusz Michalkiewicz, Jhony K Pontes, Dominic Jack, Mahsa Baktashmotlagh, and Anders Eriksson. Implicit surface representations as layers in neural networks. In *Proceedings of the IEEE/CVF International Conference on Computer Vision*, pages 4743–4752, 2019. 3
- [37] Marko Mihajlovic, Sergey Prokudin, Siyu Tang, Robert Maier, Federica Bogo, Tony Tung, and Edmond Boyer. Splatfields: Neural gaussian splats for sparse 3d and 4d reconstruction. In *European Conference on Computer Vision*, pages 313–332. Springer, 2025. 1, 2, 3
- [38] Ben Mildenhall, Pratul P Srinivasan, Rodrigo Ortiz-Cayon, Nima Khademi Kalantari, Ravi Ramamoorthi, Ren Ng, and Abhishek Kar. Local light field fusion: Practical view synthesis with prescriptive sampling guidelines. *ACM Transactions on Graphics*, 38(4):1–14, 2019. 5
- [39] Ben Mildenhall, Pratul P Srinivasan, Matthew Tancik, Jonathan T Barron, Ravi Ramamoorthi, and Ren Ng. Nerf: Representing scenes as neural radiance fields for view synthesis. In *Proceedings of the European Conference on Computer Vision*, pages 405–421. Springer, 2020. 3, 5
- [40] Patrick AP Moran. Notes on continuous stochastic phenomena. *Biometrika*, 37(1/2):17–23, 1950. 2
- [41] Thomas Müller, Alex Evans, Christoph Schied, and Alexander Keller. Instant neural graphics primitives with a multiresolution hash encoding. *ACM Trans. Graph.*, 41(4):102:1–102:15, 2022. 3
- [42] Michael Niemeyer, Lars Mescheder, Michael Oechsle, and Andreas Geiger. Occupancy flow: 4d reconstruction by learning particle dynamics. In *Proceedings of the IEEE/CVF International Conference on Computer Vision*, pages 5379–5389, 2019. 3
- [43] Michael Niemeyer, Jonathan T Barron, Ben Mildenhall, Mehdi SM Sajjadi, Andreas Geiger, and Noha Radwan. Regnerf: Regularizing neural radiance fields for view synthesis from sparse inputs. In *Proceedings of the IEEE/CVF conference on computer vision and pattern recognition*, pages 5480–5490, 2022. 3, 5
- [44] Michael Niemeyer, Fabian Manhardt, Marie-Julie Rakotosaona, Michael Oechsle, Daniel Duckworth, Rama Gosula, Keisuke Tateno, John Bates, Dominik Kaeser, and Federico Tombari. Radsplat: Radiance field-informed gaussian splatting for robust real-time rendering with 900+ fps. *arXiv preprint arXiv:2403.13806*, 2024. 3
- [45] Michael Oechsle, Lars Mescheder, Michael Niemeyer, Thilo Strauss, and Andreas Geiger. Texture fields: Learning texture representations in function space. In *Proceedings of the IEEE/CVF International Conference on Computer Vision*, pages 4531–4540, 2019. 3
- [46] Hyunwoo Park, Gun Ryu, and Wonjun Kim. Dropgaussian: Structural regularization for sparse-view gaussian splatting. In *Proceedings of the Computer Vision and Pattern Recognition Conference*, pages 21600–21609, 2025. 1, 2, 3, 5, 6
- [47] Jeong Joon Park, Peter Florence, Julian Straub, Richard Newcombe, and Steven Lovegrove. Deepsdf: Learning continuous signed distance functions for shape representation. In *Proceedings of the IEEE/CVF Conference on Computer Vision and Pattern Recognition*, pages 165–174, 2019. 3
- [48] Songyou Peng, Michael Niemeyer, Lars Mescheder, Marc Pollefeys, and Andreas Geiger. Convolutional occupancy networks. In *Proceedings of the European Conference on Computer Vision*, pages 523–540, 2020. 3
- [49] Quentin Picard, Stephane Chevobbe, Mehdi Darouich, and Jean-Yves Didier. A survey on real-time 3d scene reconstruction with slam methods in embedded systems. *arXiv preprint arXiv:2309.05349*, 2023. 3
- [50] Christian Reiser, Songyou Peng, Yiyi Liao, and Andreas Geiger. Kilonerf: Speeding up neural radiance fields with

- thousands of tiny mlps. In *Proceedings of the IEEE/CVF international conference on computer vision*, pages 14335–14345, 2021. [3](#)
- [51] Taha Samavati and Mohsen Soryani. Deep learning-based 3d reconstruction: a survey. *Artificial Intelligence Review*, 56(9):9175–9219, 2023. [1](#)
- [52] Nitish Srivastava, Geoffrey Hinton, Alex Krizhevsky, Ilya Sutskever, and Ruslan Salakhutdinov. Dropout: a simple way to prevent neural networks from overfitting. *The journal of machine learning research*, 15(1):1929–1958, 2014. [1](#)
- [53] Cheng Sun, Min Sun, and Hwann-Tzong Chen. Direct voxel grid optimization: Super-fast convergence for radiance fields reconstruction. In *Proceedings of the IEEE/CVF conference on computer vision and pattern recognition*, pages 5459–5469, 2022. [3](#)
- [54] Guangcong Wang, Zhaoxi Chen, Chen Change Loy, and Ziwei Liu. Sparsenerf: Distilling depth ranking for few-shot novel view synthesis. In *Proceedings of the IEEE/CVF International Conference on Computer Vision*, pages 9065–9076, 2023. [3](#), [5](#)
- [55] Yufeng Wang, Shuangkang Fang, Huayu Zhang, Hongguang Li, Zehao Zhang, Xianlin Zeng, and Wenrui Ding. Uav-nerf: Text-driven uav scene editing with neural radiance fields. *IEEE Transactions on Geoscience and Remote Sensing*, 2024. [3](#)
- [56] Zhou Wang, Alan C Bovik, Hamid R Sheikh, and Eero P Simoncelli. Image quality assessment: from error visibility to structural similarity. *IEEE transactions on image processing*, 13(4):600–612, 2004. [5](#)
- [57] Qiangeng Xu, Zexiang Xu, Julien Philip, Sai Bi, Zhixin Shu, Kalyan Sunkavalli, and Ulrich Neumann. Pointnerf: Point-based neural radiance fields. In *Proceedings of the IEEE/CVF conference on computer vision and pattern recognition*, pages 5438–5448, 2022. [3](#)
- [58] Yexing Xu, Longguang Wang, Minglin Chen, Sheng Ao, Li Li, and Yulan Guo. Dropouts: Dropping out gaussians for better sparse-view rendering. In *Proceedings of the Computer Vision and Pattern Recognition Conference*, pages 701–710, 2025. [1](#), [2](#), [3](#), [5](#), [6](#)
- [59] Chen Yang, Sikuang Li, Jiemin Fang, Ruofan Liang, Lingxi Xie, Xiaopeng Zhang, Wei Shen, and Qi Tian. Gaussianobject: Just taking four images to get a high-quality 3d object with gaussian splatting. *arXiv preprint arXiv:2402.10259*, 2024. [3](#)
- [60] Jiawei Yang, Marco Pavone, and Yue Wang. Freenerf: Improving few-shot neural rendering with free frequency regularization. In *Proceedings of the IEEE/CVF conference on computer vision and pattern recognition*, pages 8254–8263, 2023. [3](#), [5](#)
- [61] Zehao Yu, Anpei Chen, Binbin Huang, Torsten Sattler, and Andreas Geiger. Mip-splatting: Alias-free 3d gaussian splatting. In *Proceedings of the IEEE/CVF Conference on Computer Vision and Pattern Recognition*, pages 19447–19456, 2024. [1](#), [3](#)
- [62] Jian Zhang, Yuanqing Zhang, Huan Fu, Xiaowei Zhou, Bowen Cai, Jinchi Huang, Rongfei Jia, Binqiang Zhao, and Xing Tang. Ray priors through reprojection: Improving neural radiance fields for novel view extrapolation. In *Proceedings of the IEEE/CVF Conference on Computer Vision and Pattern Recognition*, pages 18376–18386, 2022. [3](#)
- [63] Jiawei Zhang, Jiahe Li, Xiaohan Yu, Lei Huang, Lin Gu, Jin Zheng, and Xiao Bai. Cor-gs: sparse-view 3d gaussian splatting via co-regularization. In *European Conference on Computer Vision*, pages 335–352. Springer, 2024. [1](#), [3](#), [5](#), [6](#), [7](#)
- [64] Richard Zhang, Phillip Isola, Alexei A Efros, Eli Shechtman, and Oliver Wang. The unreasonable effectiveness of deep features as a perceptual metric. In *Proceedings of the IEEE conference on computer vision and pattern recognition*, pages 586–595, 2018. [5](#)
- [65] Yulong Zheng, Zicheng Jiang, Shengfeng He, Yandu Sun, Junyu Dong, Huaidong Zhang, and Yong Du. Nexusgs: Sparse view synthesis with epipolar depth priors in 3d gaussian splatting. In *Proceedings of the Computer Vision and Pattern Recognition Conference*, pages 26800–26809, 2025. [3](#)
- [66] Zehao Zhu, Zhiwen Fan, Yifan Jiang, and Zhangyang Wang. Fsgs: Real-time few-shot view synthesis using gaussian splatting. In *European conference on computer vision*, pages 145–163. Springer, 2024. [3](#), [5](#), [6](#), [7](#)

Dropping Anchor and Spherical Harmonics for Sparse-view Gaussian Splatting

Supplementary Material

We present additional experiments and analyses to further validate the effectiveness and robustness of our proposed DropAnSH-GS. Specifically, we include: (1) extended ablation studies on the spherical harmonics (SH) dropout strategy, (2) visualizations of reconstructed 3D Gaussian scenes, (3) detailed quantitative comparisons on the Mip-NeRF 360 and Blender datasets, and (4) a discussion of potential directions for future work.

6. Additional Experimental Results

Table 8. Effect of with and without Drop SH strategy on the Blender dataset (8 views). The Drop SH strategy encourages the effective parameters to concentrate in lower-degree SH coefficients, thereby mitigating the performance degradation caused by direct SH truncation.

	PSNR \uparrow	SSIM \uparrow	LPIPS \downarrow
w/o - SH ₀	24.57	0.879	0.112
w/ - SH ₀	25.04	0.883	0.093
w/o - SH ₁	24.96	0.885	0.096
w/ - SH ₁	25.34	0.890	0.090
w/o - SH ₂	25.21	0.887	0.091
w/ - SH ₂	25.47	0.891	0.089
w/o - SH ₃	25.36	0.890	0.090
w/ - SH ₃	25.50	0.891	0.088

Additional Ablation Study. We further evaluate the impact of the Drop SH strategy on model performance under different levels of SH truncation. On the Blender dataset with 8 input views, we train two sets of models, with and without the Drop SH strategy, and truncate their SH coefficients to varying degrees during inference. The average performance metrics are summarized in Table 8. As shown, directly truncating high-degree SH coefficients significantly degrades performance when Drop SH is not applied. In contrast, models trained with Drop SH exhibit much smaller performance drops, indicating that, beyond mitigating overfitting, Drop SH effectively concentrates information in lower-degree SH components. This enables users to reduce model size via SH truncation while maintaining high rendering quality.

Visualization of the Entire Reconstruction Scene. In Figure 8, we present the reconstructed entire scenes. It can be observed that our method produces results that are more complete and natural. Our method fundamentally mitigates

the neighbor compensation effect by randomly selecting a set of “anchors” and simultaneously dropping their spatial neighbors, thereby creating larger information voids. This design encourages remaining Gaussian to rely on a more comprehensive scene context, serving as an effective form of regularization that alleviates overfitting. As a result, even when trained under sparse-view conditions, our model develops a more complete and global understanding of the scene’s geometric structure. When rendering from novel views, it can thus reconstruct more coherent and natural structures. In contrast, baseline methods tend to over-rely on local information, an approach that may work under dense-view settings but easily leads to overfitting and local artifacts when visual information is limited.

Additional Comparison Results. In Tables 9 and 10, we present supplementary quantitative results that complement those in Table 2 of the main text. These results consistently demonstrate that our method significantly outperforms existing 3DGS variants tailored for sparse-view settings, delivering both higher rendering quality and more compact model representations.

7. Discussion on Future Work

The anchor selection mechanism in our DropAnSH-GS is based on uniform random sampling. However, since the distribution of Gaussians is often non-uniform and their importance can vary across different parts of a 3D scene, exploring more sophisticated anchor selection mechanisms is a valuable direction. For instance, strategies based on gradient magnitude or opacity could be more effective, as these properties often highlight regions that are more critical during optimization. Furthermore, DropAnSH-GS selects neighbors for an anchor Gaussian based solely on the Euclidean distance between their positions. This simple spatial proximity metric, however, may not be optimal. Due to the anisotropic nature of Gaussians and the local differences of 3D scenes, physically adjacent Gaussians are not always the most functionally complementary. Therefore, designing more sophisticated neighbor selection schemes presents a promising avenue for future research. Such strategies could incorporate other factors, such as intrinsic Gaussian attributes, local scene characteristics, or even view-dependent information to better identify and regularize clusters of functionally redundant Gaussians.



original scene views



3DGS



DropoutGS



DropGaussian



Ours

Figure 8. **Visualization of the entire reconstruction scene.** Our method produces results that are more complete and natural.

Table 9. **Quantitative comparison on the MipNeRF-360 dataset (12 views).** SH_n denotes retaining only the first n degrees of SH coefficients during inference.

Methods	PSNR \uparrow	SSIM \uparrow	LPIPS \downarrow	Size (MB) \downarrow
3DGS	18.58	0.526	0.419	143.4
DNGaussian	18.84	0.543	0.468	80.7
FSGS	18.80	0.531	0.418	172.1
CoR-GS	19.42	0.556	0.418	117.4
DropoutGS	19.17	0.558	0.386	68.4
DropGaussian	19.66	0.569	0.374	120.7
Ours- SH_0	19.71	0.563	0.377	33.8
Ours- SH_1	19.86	<u>0.571</u>	0.371	<u>51.8</u>
Ours- SH_2	19.95	0.576	<u>0.363</u>	81.1
Ours- SH_3	<u>19.93</u>	0.576	0.362	122.6

Table 10. **Quantitative comparison on the Blender dataset (8 views).** SH_n denotes retaining only the first n degrees of SH coefficients during inference.

Methods	PSNR \uparrow	SSIM \uparrow	LPIPS \downarrow	Size (Mb) \downarrow
3DGS	22.13	0.855	0.132	6.5
DNGaussian	24.31	0.886	0.088	5.5
FSGS	24.64	0.895	0.095	8.4
CoR-GS	24.31	0.886	0.091	6.3
DropoutGS	24.79	0.877	0.110	5.2
DropGaussian	25.17	0.882	0.100	6.0
Ours- SH_0	25.04	0.883	0.093	1.7
Ours- SH_1	25.34	0.890	0.090	<u>2.6</u>
Ours- SH_2	<u>25.47</u>	<u>0.891</u>	<u>0.089</u>	4.1
Ours- SH_3	25.50	<u>0.891</u>	0.088	6.2